PHYSICAL REVIEW D VOLUME 22, NUMBER 11 1 DECEMBER 1980

"Soft-pion" production in the reaction $NN \to NN\pi$

J. Dubach* and R. R. Silbar
Theoretical Division, Los Alamos Scientific Laboratory, University of California, Los Alamos, New Mexico 87545

W. M. Kloet
Department of Physics and Astronomy, Rutgers University, New Brunswick, New Jersey 08903
(Received 9 June 1980)

We examine the reaction $NN \to NN\pi$ for "soft-pion" kinematics ($\vec{p}_\pi = 0$ in the center of mass). An earlier calculation based on the Adler-Dothan theorem severely underestimated the $\vec{p}_\pi = 0$ cross section for $pp \to np\pi^+$ at 740 MeV. We attempt to understand this discrepancy in the context of a relativistic, unitary, three-body isobar model. The postemission Δ-pole contributions are shown to be very important, even for these "soft-pion" kinematics. Relatively high partial waves in the $NN \to N\Delta$ isobar amplitude are significant. However, after summing all the postemission and preemission diagrams, the discrepancy with experiment is only partially removed.

I. INTRODUCTION

It is apparently not widely recognized that soft-pion techniques often predict pion-production cross sections an order of magnitude smaller than experiment. These techniques stem from a soft-pion theorem[1] based upon the concept of a partially conserved axial-vector current (PCAC). The assumptions of current algebra are not involved. The theorem says that, in the soft-pion limit (e.g., $\vec{p}_\pi \to 0$, then $m_\pi \to 0$), the pion-production amplitude is given by nucleon-pole graphs. For the process $NN \to NN\pi$ these graphs are shown in Figs. 1(a) and 1(b). Other contributions, such as the breakup of resonances [Fig. 1(c)] or internal-emission graphs [Fig. 1(d)], are of higher order in p_π and, presumably, small. The amplitude given by the pole graphs of Figs. 1(a) and 1(b) is to be calculated using axial-vector $NN\pi$ coupling at the vertex. Further, the blobs representing $NN \to NN$ scattering are to be evaluated on shell.

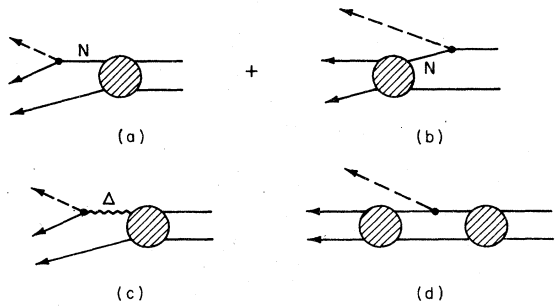

FIG. 1. (a) and (b) Nucleon-pole graphs, presumed to be dominant in the soft-pion limit; (c) breakup of the Δ, or (3,3) resonance; (d) internal emission graph.

This procedure is similar to calculations using the low-energy photon theorem for NN bremsstrahlung.[2]

The calculation outlined above for $NN \to NN\pi$ was carried out more than ten years ago[3] in anticipation of an experiment that would measure the "soft-pion" production cross section.[4] For physical pions ($m_\pi \equiv \mu \neq 0$) there is some ambiguity as to what kinematic situation best corresponds to the soft-pion limit. A common choice has been the limit in which $\vec{p}_\pi = 0$ in the center-of-mass frame. This prescription was followed in Ref. 3.

The experimental $pp \to np\pi^+$ cross section at $T_{\rm Lab} = 740$ MeV was subsequently found[4] to be about 8 times larger than the soft-pion predictions (for $T_{\pi,\rm c.m.} \lesssim 30$ MeV). Since the NN phase shifts in the energy region of interest were not too well known at the time the calculations of Ref. 3 were done, we repeated these calculations using more recent phase shifts.[5] We found that the predicted $\vec{p}_\pi = 0$ cross section changed by less than 20% and the serious discrepancy remains.

One suggestion[6] made for understanding this situation was that the contributions of the Δ isobar [Fig. 1(c)] were non-negligible for "soft" but physical pions. In particular, the kinematical situation with $\vec{p}_\pi = 0$ enhances contributions from the higher $N\Delta$ partial waves. Reference 6 showed that a crude extension of the Mandelstam isobar model[7] to include a small d-wave contribution could predict a cross section in agreement with experiment.

Since that time soft-pion calculations for several other production processes have also predicted cross sections much smaller than experiment. These studies include the reactions $\bar{p}p \to \bar{N}N\pi$,[8] $\bar{\Lambda}\Lambda\pi\pi$,[9,10] and $\bar{K}K\bar{K}K\pi\pi$.[11] In each case it is quite likely that, apart from the leading pole

diagrams, there are large contributions ("background terms") from resonances, such as N^*, Δ, Y^*, or K^*.

The present paper considers the importance of resonance contributions, for "soft-pion" kinematics, in a specific model for the $NN \to NN\pi$ reaction. This investigation emerges naturally from recent nucleon-nucleon dynamical calculations at intermediate energies.[12-14] The model, which assumes the isobar breakup mechanism (Fig. 2), gives a *total* pion production cross section in good agreement with experiment. (There are essentially no free parameters in the calculation reported in Ref. 12.) We thus consider the $\vec{p}_\pi = 0$ ("soft-pion") limit of this model to determine more precisely how Δ resonances enter this special kinematic situation and whether their role is as important as conjectured in Ref. 6. It turns out that at 800 MeV, inclusion of the postemission Δ-resonance contributions gives a cross section 4 times larger than that using postemission nucleon-pole terms alone. Moreover, as Ref. 6 suggested, many high partial waves are involved.

However, in many applications of the soft-pion theorem, preemission nucleon-pole graphs [Fig. 1(b)] are found to be larger than the postemission nucleon-pole graphs. Thus, to give a full discussion of the $\vec{p}_\pi = 0$ cross section, we have extended our calculation to include such graphs, even though this procedure may deviate from the spirit of the three-body model. The isobar amplitudes needed in the preemission graphs are again taken from our three-body model. The inclusion of the preemission graphs brings the predicted $\vec{p}_\pi = 0$ cross section to within a factor of 3 or so of the experimental value. The difficulty we have in reproducing the experimental cross section at $\vec{p}_\pi = 0$ may therefore be an indication that the dynamics in the "soft-pion" kinematic region is more complicated than has been suggested in the past.

It is useful to put the Δ-pole corrections to the soft-pion $NN \to NN\pi$ into context with other soft-pion current-algebra calculations. Significant Δ-pole contributions have also been found in elastic πN scattering,[15,16] nonleptonic hyperon decays,[17] and photoproduction of pions from nucleons.[18] Typically, these "hard-pion corrections" have been of the order of 20 to 30%, and it has always been the case that they have improved the agreement between theory and experiment. What is remarkable about the $NN \to NN\pi$ case discussed here is that the Δ-pole corrections are quite large (~50%). Unfortunately, the Δ-pole graphs do not completely remove the discrepancy between the large experimental $\vec{p}_\pi = 0$ cross section and the prediction based on the soft-pion theorem.

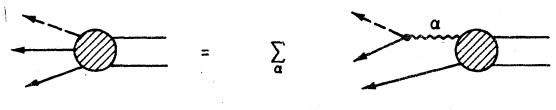

FIG. 2. Two-to-three-body $NN \to NN\pi$ amplitude in the isobar model. Here the sum on α includes the $N' \equiv P_{11}$ and $\Delta \equiv P_{33}$ πN isobars (quasiparticles).

This paper is organized as follows. Section II gives the derivation of the amplitude and cross section for $NN \to NN\pi$ at $\vec{p}_\pi = 0$, in the isobar model. The numerical comparison of the Δ and nucleon postemission graphs is discussed in Sec. III. Section IV presents the details needed to include preemission graphs in the calculation. The results of the complete calculation are discussed in Sec. V, and Sec. VI summarizes our conclusions.

II. AMPLITUDE AND CROSS SECTION IN THE ISOBAR MODEL

A. Amplitude

In the isobar model, the two-to-three-body amplitude for $NN \to NN\pi$ is given (schematically) by

$$\langle NN\pi | T | NN \rangle = \sum_\alpha g_\alpha v_\alpha G_\alpha^{(2)} T_\alpha , \tag{1}$$

where the index α runs over the isobars (or quasiparticles) in the model. Equation (1) is depicted graphically in Fig. 2. Here g_α and v_α are the coupling constant and vertex function (including all spin complications) for the $\alpha \to N\pi$ vertex, $G_\alpha^{(2)}$ is the two-body propagator for the (sometimes resonant) πN state α represented by the wavy line, and T_α is the $NN \to N\alpha$ isobar amplitude.

If we restrict α to N' and Δ, i.e., πN interactions in the P_{11} and P_{33} partial waves, respectively, then the vertices, propagators, and isobar amplitudes are all specified in terms of the unitary, relativistic three-body model described in detail in Ref. 13. Our discussion of the g_α, v_α, $G_\alpha^{(2)}$, and T_α will follow that reference closely.

Figure 3 shows the labeling of the two-to-three amplitude with respect to (center-of-mass) momenta and spin and isospin quantum numbers. The $\alpha \to N\pi$ vertex for $\alpha = N', \Delta$ can be written as

$$\langle \pi N | \alpha \rangle \equiv \langle \vec{p}_\pi = 0, t'_\pi; -\vec{p}', m'_2, t'_2 | \alpha; -\vec{p}', m'_\alpha, t'_\alpha \rangle$$

$$= F_\alpha(p') \begin{pmatrix} \frac{1}{2} & 1 & i_\alpha \\ t'_2 & t'_\pi & t'_\alpha \end{pmatrix} \begin{pmatrix} \frac{1}{2} & 1 & s_\alpha \\ m'_2 & \lambda' & m'_\alpha \end{pmatrix} Y_{1\lambda'}(\hat{p}') , \tag{2}$$

where F_α contains everything that does not depend upon direction or spin and isospin components.

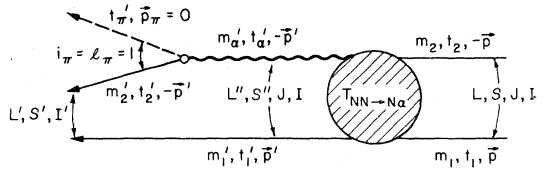

FIG. 3. Quantum numbers and labeling of a general isobar-breakup graph. The spin projection of the isobar, m_α', must be summed over in calculating the amplitude.

[We will also include the $G_\alpha^{(2)}(p')$ as a factor in it]. This simple form results from the assumption $\vec{p}_\pi = 0$. From Ref. 13, Eq. (5.5),

$$F_N(p') = 3g_N v_N(V'^2)N(E', m)N(\mathcal{E}', M) \times p'\left(\frac{1}{\mathcal{E}'+M'} - \frac{1}{E'+m}\right)G_N^{(2)}(p'), \qquad (3)$$

where

$$M'^2 \equiv \sigma' = (P - p_1')^2 = W^2 - 2WE' + m^2 = (p_2' + p_\pi)^2 = m^2 + 2\mu E' + \mu^2 \geq (m+\mu)^2,$$

$$\mathcal{E}' = (M'^2 + p'^2)^{1/2}, \quad E' = (m^2 + p'^2)^{1/2},$$

$$W^2 = 4m^2 + 2mT_{\text{lab}}, \quad p' = [\tfrac{1}{4}(W-\mu)^2 - m^2]^{1/2},$$

$$N(E, m) = [(E+m)/2m]^{1/2}, \quad v_N(V'^2) = \exp[-\tfrac{1}{2}V'^2/\beta_N^2],$$

$$V' = \mu p'/M', \quad g_N = 13.41, \quad \beta_N = 1.75 \text{ GeV}.$$

Likewise,

$$F_\Delta(p') = g_\Delta v_\Delta(V'^2)N(E', m)N(\mathcal{E}', M')(p'/M')G_\Delta^{(2)}(p'), \qquad (4)$$

where

$$v_\Delta(V'^2) = \beta_\Delta^2/(\beta_\Delta^2 + V'^2), \quad g_\Delta = 2.43, \quad \beta_\Delta = 0.46 \text{ GeV}.$$

[In these expressions we have suppressed a factor of $(4\pi/3)^{1/2}$ which eventually will be canceled when we use the addition theorem for spherical harmonics.] The vertices here differ slightly from the expressions in Ref. 13 in that there we took $M' = m$ or M_Δ, independent of p'. The reason for this choice in Ref. 13 was to avoid complex values for $N(\mathcal{E}', M')$ when doing the integrations required to solve the coupled three-body equations for the T_α. Here, however, it is more appropriate that M' be the invariant mass of the πN system [particularly since $M' = m$ would, by Eq. (3), mean $F_N = 0$].

The propagators $G_\alpha^{(2)}(p')$ differ only by a factor from the three-body propagators that appear in the integral equations for the T_α,

$$G_\alpha^{(2)}(p') = (2m)^{-1}G_\alpha^{(3)}(p') = -1/D_\alpha(\sigma'), \qquad (5)$$

where the D functions are discussed in detail in Sec. IV of Ref. 13. For $\sigma' > (m+\mu)^2$, these functions are complex, reflecting the two-particle unitarity cut. The P_{11} propagator $G_N^{(2)}$ has a nucleon pole at $\sigma' = m^2$, and $G_\Delta^{(2)}$ resembles a Breit-Wigner resonance factor.

With Eq. (2), the contribution of isobar α to the two-to-three amplitude is

$$\langle NN\pi|T_\alpha|NN\rangle = F_\alpha \sum_{m_\alpha'} \begin{pmatrix} \frac{1}{2} & 1 \\ t_2' & t_\pi' \end{pmatrix} \begin{pmatrix} i_\alpha \\ t_\alpha' \end{pmatrix} \begin{pmatrix} \frac{1}{2} & 1 \\ m_2' & \lambda' \end{pmatrix} \begin{pmatrix} s_\alpha \\ m_\alpha' \end{pmatrix} Y_{1\lambda'}(p') \langle N\alpha; \vec{p}'\, m_1' t_1', -\vec{p}'\, m_\alpha' t_\alpha' | T | NN; \vec{p} m_1 t_1, -\vec{p} m_2 t_2\rangle$$

$$= F_\alpha(p') \sum_{LS, L''S'', JI} \begin{pmatrix} \frac{1}{2} & 1 \\ t_2' & t_\pi' \end{pmatrix} \begin{pmatrix} i_\alpha \\ t_\alpha' \end{pmatrix} \begin{pmatrix} \frac{1}{2} & i_\alpha \\ t_1' & t_2' \end{pmatrix} \begin{pmatrix} I \\ M_I \end{pmatrix} \begin{pmatrix} \frac{1}{2} & \frac{1}{2} \\ t_1 & t_2 \end{pmatrix} \begin{pmatrix} I \\ M_I \end{pmatrix}$$

$$\times \sum_{M,\lambda} \begin{pmatrix} \frac{1}{2} & 1 \\ m_2' & \lambda' \end{pmatrix} \begin{pmatrix} s_\alpha \\ m_2' \end{pmatrix} \begin{pmatrix} \frac{1}{2} & s_\alpha \\ m_1' & m_\alpha' \end{pmatrix} \begin{pmatrix} S'' \\ \sigma'' \end{pmatrix} \begin{pmatrix} L'' & S'' \\ \mu'' & \sigma'' \end{pmatrix} \begin{pmatrix} J \\ M \end{pmatrix} Y_{1\lambda'}(\hat{p}') Y_{L''\mu''}(\hat{p}')$$

$$\times \begin{pmatrix} \frac{1}{2} & \frac{1}{2} \\ m_1 & m_2 \end{pmatrix} \begin{pmatrix} S \\ \sigma \end{pmatrix} \begin{pmatrix} L & S \\ \mu & \sigma \end{pmatrix} \begin{pmatrix} J \\ M \end{pmatrix} Y_{L\mu}^*(\hat{p}) \langle N\alpha, p', L''S''JI | T | NN, p, LSJI\rangle, \qquad (6)$$

where, in the second equality, we have used the partial-wave decomposition [Ref. 13, Eq. (3.1)] of the isobar amplitude with quantum-number labels as indicated in Fig. 3.

The amplitude in Eq. (6) needs to be antisymmetrized with respect to the initial and final nucleons. As written, however, the expression is quite unsymmetric in the final nucleons. Using standard angular-momentum techniques,[19] we can eventually rewrite Eq. (6) in the form

$$\langle NN\pi|T_\alpha|NN\rangle = \sum_{LSI, L'S'I'J} C_J^\alpha(LSI, L'S'I')B(t_1t_2I, t_1't_2'I')A_J(m_1m_2LS, \hat{p}; m_1'm_2'L'S', \hat{p}'), \qquad (7)$$

where the isospin is contained in

$$B(t_1 t_2 I, t_1' t_2' I') = \begin{pmatrix} \frac{1}{2} & \frac{1}{2} & I \\ t_1 & t_2 & M_I \end{pmatrix} \begin{pmatrix} \frac{1}{2} & \frac{1}{2} & I' \\ t_1' & t_2' & M_I' \end{pmatrix}, \tag{8}$$

the spin and geometry is contained in

$$A_J = \sum_M A^*_{JM}(m_1 m_2 LS, \hat{p}) A_{JM}(m_1' m_2' L'S', \hat{p}'),$$
$$A_{JM}(m_1 m_2 LS, \hat{p}) = \begin{pmatrix} \frac{1}{2} & \frac{1}{2} & S \\ m_1 & m_2 & \sigma \end{pmatrix} \begin{pmatrix} L & S & J \\ \mu & \sigma & M \end{pmatrix} Y_{L\mu}(\hat{p}), \tag{9}$$

and all the dynamics are contained in

$$C_J^\alpha(LSI, L'S'I') = F_\alpha(p')(-1)^{I+J} \hat{I}_\alpha \hat{S}_\alpha \hat{I}' \hat{S}' \begin{Bmatrix} \frac{1}{2} & \frac{1}{2} & I' \\ 1 & I & I_\alpha \end{Bmatrix} \begin{pmatrix} I' & 1 & I \\ M_I' & t_\pi' & M_I \end{pmatrix}$$
$$\times \sum_{L'', S''} (-1)^{L''} \hat{L}'' \hat{S}'' \begin{pmatrix} 1 & L'' & L' \\ 0 & 0 & 0 \end{pmatrix} \begin{Bmatrix} \frac{1}{2} & \frac{1}{2} & S' \\ 1 & S'' & s_\alpha \end{Bmatrix} \begin{Bmatrix} L'' & 1 & L' \\ S' & J & S'' \end{Bmatrix} \langle N\alpha, p', L''S'' JI | T | NN, p, LSJI \rangle, \tag{10}$$

with $\hat{a} \equiv (2a+1)^{1/2}$. The C_J^α are complex quantities because of the D function (in F_α) and the partial-wave isobar amplitude T_α.

The amplitude in Eq. (7) corresponds to just one of four contributing graphs for the $NN \to NN\pi$ process, that with external legs labeled as in Fig. 3. There are three other topologically distinct graphs that must be included, together with appropriate signs to ensure the antisymmetry with respect to the initial and final NN states. Because of the symmetry properties of B and A_{JM}, the inclusion of these other three graphs is straightforward. The final form of the two-to-three-body amplitude in the isobar model is

$$\langle NN\pi | T | NN \rangle = 4 \sum_{\substack{LSI, L'S'I' \\ J}} P(LSI) P(L'S'I') C_J(LSI, L'S'I') B(t_1 t_2 I, t_1' t_2' I') A_J(m_1 m_2 LS, \hat{p}; m_1' m_2' L'S', \hat{p}'), \tag{11}$$

where the factor of 4 results from using the projection operators $P(LSI)$ defined by

$$P(LSI) = \tfrac{1}{2}[1 - (-1)^{L+S+I}]. \tag{12}$$

The $C_J(LSI, L'S'I')$ in Eq. (11) is the sum of the C_J^α, $\alpha = N$ and Δ, given by Eq. (10).

B. Cross section

The total cross section for producing pions with $\vec{p}_\pi = 0$ requires summing and averaging over final and initial spin projections and integration over all directions of the final nucleon momentum $\vec{p}'$. It is also convenient (though not strictly necessary) to average over the initial direction $\hat{p}$. Further, for a given process with fixed isospin components M_I, M_I', we sum and average over the possible isospin projections for the initial and final nucleons. Thus

$$|T_{NN \to NN\pi}|^2_{\text{ave}} = \frac{1}{n_{\text{iso}}} \frac{1}{4} \frac{1}{4\pi} \sum_{\substack{t_1 t_2 m_1 m_2 \\ t_1' t_2' m_1' m_2'}} \int d\Omega_p \int d\Omega_{p'} |\langle NN\pi | T | NN \rangle|^2, \tag{13}$$

where n_{iso} is the number of ways t_1 and t_2 can be chosen so that $t_1 + t_2 = M_I$. Substituting Eq. (12) in Eq. (13) and using orthogonality relations for the JM, P's, and B's, we find

$$|T_{NN \to NN\pi}|^2_{\text{ave}} = \frac{1}{n_{\text{iso}} \pi} \sum_{\substack{LSI, L'S'I' \\ J}}'' (2J+1) |C_J(LSI, L'S'I')|^2. \tag{14}$$

This result only depends on the dynamical quantities C_J. The double prime on the summation sign restricts $L+S+I$ and $L'+S'+I'$ to odd values only. For the process $pp \to np\pi^+$, to which we restrict our attention from now on, $n_{\text{iso}} = 1$ and $I = 1$.

The $\vec{p}_\pi = 0$ cross section can now be obtained by integrating the invariant $|T|^2_{\text{ave}}$ over phase space and dividing by the incident flux. (There is an

additional factor of $\frac{1}{2}$ because of the identical nucleons in the final state). We finally obtain

$$\frac{d\sigma}{p_\pi^{\,2}\,dp_\pi} = \frac{1}{(2\pi)^5}\,\frac{p'}{p}\,\frac{m^4}{\omega W(W-\omega)} \times \sum_{LS,L'S'I'}{}'' \sum_J (2J+1)\,|C_J(LSI,L'S'I')|^2, \tag{15}$$

where ω is the total pion energy in the center of mass. In this equation we have taken the rapid dependence on p_π, which comes from the pion phase-space factor, over to the left-hand side.

III. ISOBAR-MODEL RESULTS

In the calculations presented here we have used the isobar amplitudes T_α obtained from the unitary, relativistic three-body model of Ref. 13. The coupled Blankenbecler-Sugar integral equations for T_N and T_Δ, depicted in Fig. 4, have one-pion-exchange (OPE) Born terms as driving terms. These equations are solved for the partial-wave amplitudes by iterating and forming Padé approximants from the iterates.

The functions F_N and F_Δ have only small imaginary parts, since M', the energy in the πN center of mass, is so close to the threshold at $m+\mu$. Their magnitudes are plotted as solid lines in Fig. 5 as a function of laboratory kinetic energy of the incident proton. (The curves labeled $F_{N,\mathrm{pre}}$ and $F_{\Delta,\mathrm{pre}}$ will be discussed in Sec. V). Even near threshold, F_Δ is comparable to F_N, but above 1000 MeV F_Δ becomes substantially larger. Its steep rise as a function of T_{lab} reflects the onset of the (3, 3) resonance. (F_Δ will continue to rise until the resonance pole is reached at $T_{\mathrm{lab}} \cong 9$ GeV).

The individual contributions of the J^p partial waves (J^p is the total angular momentum and parity of the initial NN state) to the "soft-pion" cross section $d\sigma/p_\pi^{\,2}dp_\pi$ are shown in Fig. 6 for $pp \to np\pi^+$ for two incident energies. The separate contributions of the N-pole graphs (σ_N) and Δ-pole graphs (σ_Δ) are also shown. There is often a great deal of interference between these two contributions, which is reflected in the fact that $\sigma_{\mathrm{tot}} \neq \sigma_N + \sigma_\Delta$. Besides noting that many partial waves contribute to σ_{tot}, we observe the following:

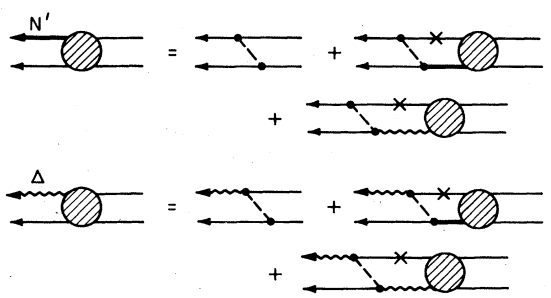

FIG. 4. Coupled Blankenbecler-Sugar integral equations for the $NN \to NN'$ and $NN \to N\Delta$ isobar amplitudes.

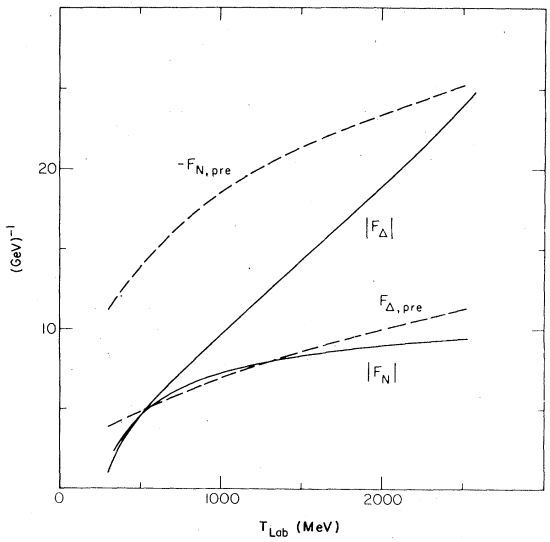

FIG. 5. Energy dependence of the F_α defined in Eqs. (3), (4), (17), and (18).

(1) The $J^p = 2^+$, or $^1D_2$, partial wave gives a relatively small contribution, despite the usual expectation that $NN(^1D_2) \to N\Delta(^5S_2)$ is a channel favored by angular-momentum barrier factors, and thus is expected to be important. This, however, is not the case, because the relative $N\Delta$ momentum p' is quite large for $\vec{p}_\pi = 0$.

(2) The largest $NN \to N\Delta$ contributions are in the "triplet-odd" ($L = J = \mathrm{odd}$, $S = 1, I = 1$) partial waves. Even the 7^- state, for which the $N\Delta$ state has relative orbital angular momentum $L \geq 5$, contributes more than 2% of the total "soft-pion" cross section at 800 MeV.

(3) In all partial waves but one ($J^p = 2^-$), the nucleon-pole contribution, which is supposedly dominant in the soft-pion limit, is small compared with the Δ-pole contribution.

(4) The relative importance of the Δ-pole vis-a-vis the N-pole contributions grows as the energy increases, as expected from the behavior of the F_α as plotted in Fig. 5.

(5). The relative importance of the higher partial waves also grows as the energy increases.

Figure 7 shows the sums of all the separate J^p partial-wave contributions as functions of incident energy. Again, the Δ-pole contribution dominates the N-pole contribution at all energies. In particular, at 740 MeV, the cross section including the Δ-pole contribution is 3.6 times larger

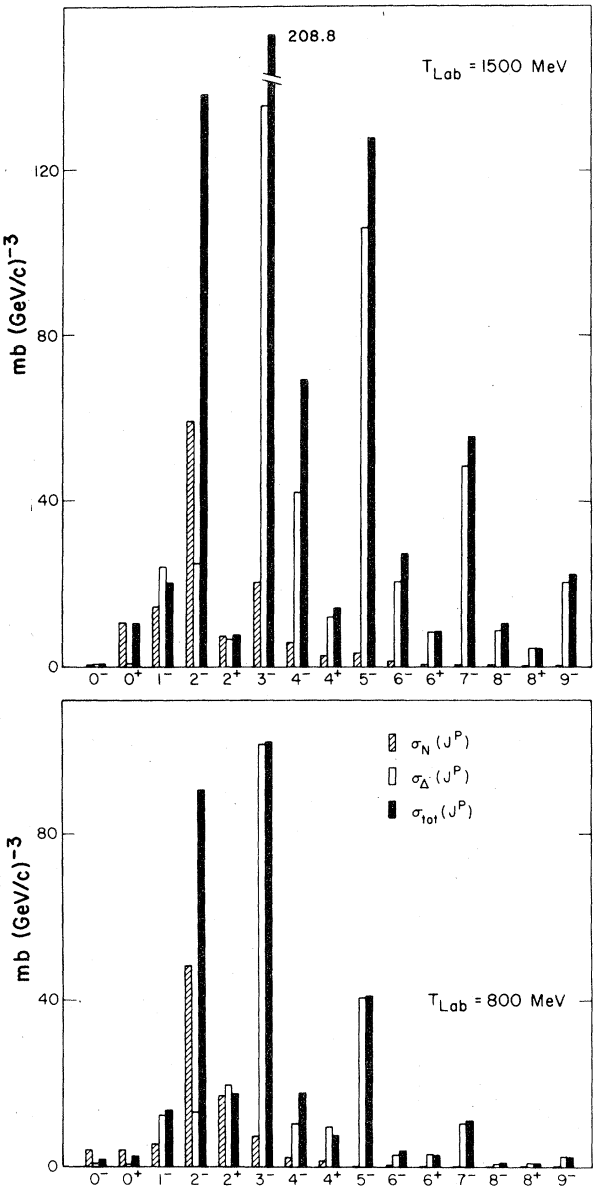

FIG. 6. Contributions of the individual partial-wave amplitudes to the $pp \to np\pi^+$ "soft-pion" ($\vec{p}_\pi = 0$) cross section at $T_{lab} = 800$ and 1500 MeV. The contributions of the N' and Δ' postemission graphs are shown separately, along with their sum.

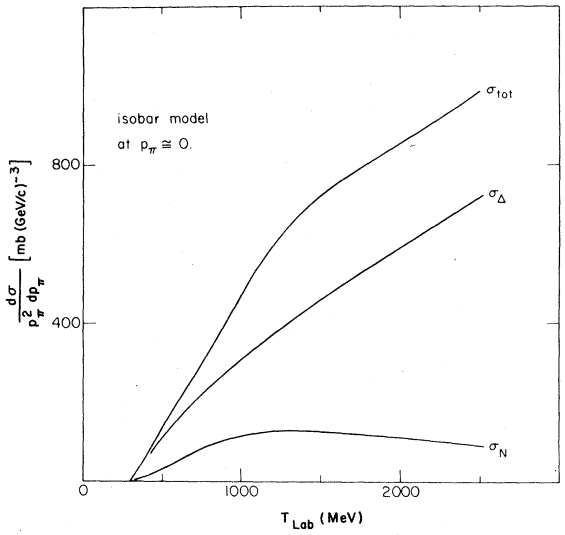

FIG. 7. The isobar-model prediction for the $\vec{p}_\pi = 0$ $pp \to np\pi^+$ cross section as a function of incident kinetic energy. The experimental cross section (Ref. 4) is much larger, 2500 mb (GeV/c)$^{-3}$ at 740 MeV.

than that from the N-pole graph alone.[20]

However, the predicted isobar model cross section for $\vec{p}_\pi = 0$ is quite small compared with the experimental value. From Ref. 4, the $d\sigma/p_\pi{}^2 dp_\pi$ at 740 MeV is about 2500 mb/(GeV/c)^3, nine times larger than shown in Fig. 7. To a large extent, this discrepancy is due to the lack of preemission nucleon-pole graphs [(Fig. 1(b)] in the isobar model. In checking the calculation of Ref. 3, we found that the preemission N-pole graphs contribute three times as much to the predicted $pp \to np\pi^+$ cross section as the postemission graphs. Therefore, in the next section we will consider the contribution of graphs such as that in Fig. 1(b).

IV. INCLUSION OF PRE-EMISSION GRAPHS

Figure 8 shows the nucleon and Δ preemission graphs that we consider in this section. These graphs do not in fact appear in the isobar model described in Ref. 13. If that model were to include a nucleon-nucleon quasiparticle interaction, one could generate the nucleon preemission graph, but the Δ preemission graph would never appear in a three-body $NN\pi$ model. We will use the isobar model of Ref. 13 merely to evaluate the $N\alpha \to NN$ amplitude that occurs in the preemission graph of Fig. 8. As a caveat, note that a piece of the nucleon preemission graph contains the u-channel nucleon pole contribution to the $\pi N \to \pi N$

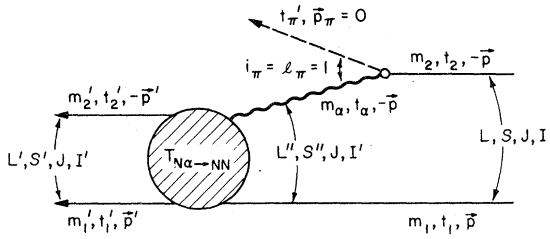

FIG. 8. Quantum numbers and labeling for a general preemission graph.

amplitude. This is presumably the dynamical mechanism responsible for generating the P_{33} πN resonance. Therefore, one might worry that there is some double counting when both nucleon preemission and Δ postemission are included. Nonetheless, it is instructive to see how the $\vec{p}_\pi = 0$ cross-section predictions change when preemission graphs are included.

We can again manipulate the preemission graph, labeled as in Fig. 8, into the form of Eq. 7, but with a different dynamical quantity $C^\alpha_{J,\mathrm{pre}}$, in place of C^α_J. The $N \to \alpha\pi$ vertex is of the form

$$\langle \pi\alpha | N\rangle = \langle \vec{p}_\pi = 0, t'_\pi; \alpha, -\vec{p}, m_\alpha, t_\alpha | N; -\vec{p}, m_2, t_2\rangle$$

$$= F_{\alpha,\mathrm{pre}}(p) \begin{pmatrix} i_\alpha & 1 \\ t_\alpha & t'_\pi \end{pmatrix} \Big| \begin{matrix} \frac{1}{2} \\ t_2 \end{matrix} \begin{pmatrix} s_\alpha & 1 \\ m_\alpha & \lambda' \end{pmatrix} \Big| \begin{matrix} \frac{1}{2} \\ m_2 \end{matrix} Y_{1\lambda'}(\hat{p})$$

$$= (-1)^{t'_\pi} 2(\hat{i}_\alpha \hat{s}_\alpha)^{-1} F_{\alpha,\mathrm{pre}}(p) \begin{pmatrix} \frac{1}{2} & 1 \\ t_2 & -t'_\pi \end{pmatrix} \Big| \begin{matrix} i_\alpha \\ t_\alpha \end{matrix} \begin{pmatrix} \frac{1}{2} & 1 \\ m_2 & \lambda \end{pmatrix} \Big| \begin{matrix} s_\alpha \\ m_\alpha \end{matrix} Y^*_{1\lambda}(\hat{p}), \tag{16}$$

where we have used $i_\alpha = s_\alpha$. The F's are

$$F_{N,\mathrm{pre}}(p) = 3 g_N v_N(V^2) N(E,m) N(\mathcal{E},M) p \left(\frac{1}{E+m} - \frac{1}{\mathcal{E}+M} \right) G^{(2)}_N(p), \tag{17}$$

$$F_{\Delta,\mathrm{pre}} = \sqrt{2}\, g_\Delta v_\Delta(V^2) N(E,m) N(\mathcal{E},M) p\, G^{(2)}_\Delta(p), \tag{18}$$

where

$$\mathcal{E} = (M^2 + p^2)^{1/2}, \quad E = (m^2 + p^2)^{1/2}, \quad V = \mu p/m,$$

$$M^2 \equiv \sigma = (P - p_1 - p_\pi)^2 = (W-\mu)^2 - 2(W-\mu)E + m^2 = (p_2 - p_\pi)^2 = m^2 - 2\mu E + \mu^2 \leq (m-\mu)^2.$$

Thus,

$$\langle NN\pi | T_{\alpha,\mathrm{pre}} | NN\rangle = F_{\alpha,\mathrm{pre}} \sum_\lambda \begin{pmatrix} \frac{1}{2} & 1 \\ t_2 & -t'_\pi \end{pmatrix} \Big| \begin{matrix} i_\alpha \\ t_\alpha \end{matrix} \begin{pmatrix} \frac{1}{2} & 1 \\ m_2 & \lambda \end{pmatrix} \Big| \begin{matrix} s_\alpha \\ m_\alpha \end{matrix} Y^*_{1\lambda}(\hat{p})$$

$$\times \langle NN; \vec{p}\,' m'_1 t'_1, -\vec{p}\,' m'_2 t'_2 | T | N\alpha; \vec{p}\, m_1 t_1, -\vec{p} m_\alpha t_\alpha\rangle. \tag{19}$$

In contrast with the isobar amplitude in Eq. (7), which has the right side on the mass shell, here the left side of the isobar amplitude (the final NN state) is on shell. To relate this to the isobar amplitudes that we calculate in Ref. 13, we use time-reversal invariance. With phases as given in Ref. 19, Eq. (2.8.2), we find, after some algebra,

$$\langle NN; \vec{p}\,' m'_1 t'_1, -\vec{p}\,' m'_2 t'_2 | T | N\alpha; \vec{p} m_1 t_1, -\vec{p} m_\alpha t_\alpha\rangle = \langle NN; -\vec{p}\,' m'_1 t'_1, \vec{p}\,' m'_2 t'_2 | T | N\alpha; -\vec{p} m_1 t_1, \vec{p} m_\alpha t_\alpha\rangle^*$$

$$= (-1)^{m'_1 + m'_2 + m_1 + m_\alpha + t'_1 + t'_2 + t_1 + t_\alpha}$$

$$\times \langle N\alpha; -\vec{p} - m_1 - t_1, \vec{p} - m_\alpha - t_\alpha | T | NN; -\vec{p}\,' - m'_1 - t'_1, \vec{p}\,' - m'_2 - t'_2\rangle$$

$$= \sum_{L'S', L''S''JI'} \sum_M \begin{pmatrix} \frac{1}{2} & \frac{1}{2} \\ m'_1 & m'_2 \end{pmatrix} \Big| \begin{matrix} S' \\ \sigma' \end{matrix} \begin{pmatrix} L' & S' \\ \mu' & \sigma' \end{pmatrix} \Big| \begin{matrix} J \\ M \end{matrix} \begin{pmatrix} \frac{1}{2} & \frac{1}{2} \\ t'_1 & t'_2 \end{pmatrix} \Big| \begin{matrix} I' \\ M'_I \end{matrix} Y_{L'\mu'}(\hat{p}')$$

$$\times \begin{pmatrix} \frac{1}{2} & s_\alpha \\ m_1 & m_2 \end{pmatrix} \Big| \begin{matrix} S'' \\ \sigma'' \end{matrix} \begin{pmatrix} L'' & S'' \\ \mu'' & \sigma'' \end{pmatrix} \Big| \begin{matrix} J \\ M \end{matrix} \begin{pmatrix} \frac{1}{2} & i_\alpha \\ t_1 & t_2 \end{pmatrix} \Big| \begin{matrix} I' \\ M'_I \end{matrix} Y^*_{L''\mu''}(\hat{p})$$

$$\times \langle N\alpha; p, L''S''JI' | T | NN, p', L'S'JI'\rangle. \tag{20}$$

The partial-wave amplitudes here are to be evaluated at an energy $T_{\mathrm{lab},\mathrm{pre}}$ corresponding to an on-the-energy-shell NN center-of-mass momentum p'.

Substituting Eq. (20) into Eq. (19), and then carrying out some angular-momentum algebra, we can con-

vert $\langle NN\pi|T_{\alpha,\,\mathrm{pre}}|NN\rangle$ to the form of Eq. (7), but with

$$C^{\alpha}_{J,\,\mathrm{pre}}(LSI,L'S'I')=F_{\alpha,\,\mathrm{pre}}(p)(-1)^{t'_\pi+I'+J}2\hat{I}\hat{S}\begin{Bmatrix}\frac{1}{2} & \frac{1}{2} & I\\ 1 & I' & i_\alpha\end{Bmatrix}\begin{pmatrix}I & 1 & I'\\ M_I & -t'_\alpha & M'_I\end{pmatrix}$$

$$\times\sum_{L'',\,S''}(-1)^{L''}\hat{L}''\hat{S}''\begin{pmatrix}1 & L'' & L\\ 0 & 0 & 0\end{pmatrix}\begin{Bmatrix}\frac{1}{2} & \frac{1}{2} & S\\ 1 & S'' & s_\alpha\end{Bmatrix}\begin{Bmatrix}L'' & 1 & L\\ S & J & S''\end{Bmatrix}$$

$$\times\langle N\alpha,p,L''S''JI'|T|NN,p',L'S'JI'\rangle\,. \tag{21}$$

Thus, the form of the "soft-pion" production cross section is still given by Eq. (15), but with

$$C_J(LSI,L'S'I')=C^N_J+C^\Delta_J+C^N_{J,\,\mathrm{pre}}+C^\Delta_{J,\,\mathrm{pre}}\,. \tag{22}$$

V. RESULTS INCLUDING PREEMISSION

The quantities $F_{N,\,\mathrm{pre}}$ and $F_{\Delta,\,\mathrm{pre}}$ (which are real, since M is less than the πN threshold at $m+\mu$) are also plotted in Fig. 5 as dashed curves. The $F_{N,\mathrm{pre}}$ is even larger than $|F_\Delta|$, indicating why nucleon preemission is so important for soft-pion kinematics.

Figure 9 shows plots of how the four components of a number of the C_J's compare with one another in the complex plane. The nucleon preemission and postemission contributions, in this model, are generally of the same size as Δ postemission,

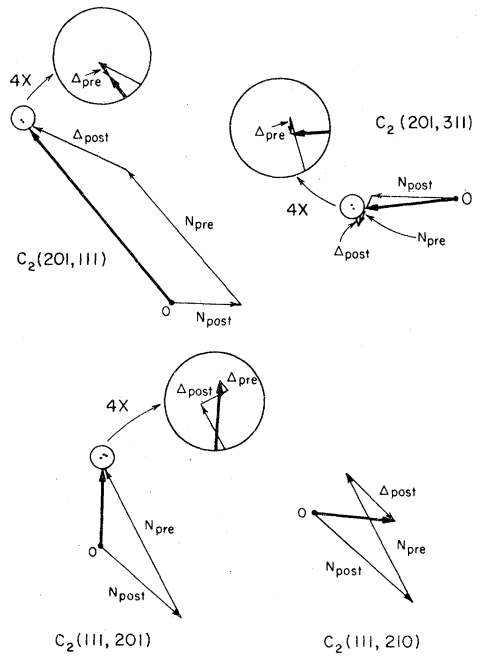

FIG. 9. Contributions of different graphs to selected $C_J(LSI,\,L'S'I')$ at $T_{\mathrm{lab}}=800$ MeV. The total $\vec{p}_\pi=0$ cross section sums over squared magnitudes of these C_J [Eq. (15)].

while Δ preemission is nearly always small. The following remarks can be made.

(1) When the initial NN state is in a "singlet-even" partial wave ($L=J=$ even, $S=0$, $I=1$), the final NN state necessarily has unique isospin $I'=1$. This is because the final NN state has odd parity following the pion emission. Similarly, for a "triplet-odd" initial state, I' can only be 0. Only for the "triplet-even" initial state ($L=J\pm1$, $J=$ even, $S=1, I=1$), do final NN states of different isospin I' come in (but without interfering).

(2) As a corollary to the above, $I'=1$ "triplet-odd" and $I'=0$ "singlet-odd" NN final-states interactions never contribute to the nucleon preemission graphs.

(3) For final NN states with $I'=0$, there is no Δ preemission contribution.

(4) For the preemission graphs, which have a large value of relative momentum p between the isobar and the spectator nucleon, the angular-momentum barrier arguments are even less applicable than in postemission. For example, the small Δ preemission contribution to $C_2(111,201)$ comes about because of a cancellation between the ${}^5S_2$, ${}^3D_2$, and ${}^5D_2$ $N\Delta$ partial waves.

The contributions to the total soft-pion production cross section from the separate partial waves are again shown, at 800 MeV, in Fig. 10. Only for the 0^- initial NN state does Δ preemission make a non-negligible contribution. The nucleon preemission contribution is largest in the 1^- and 2^- partial waves. Finally, as in Fig. 6, there is quite a lot of interference between the different pieces of the total amplitude.

The total $\vec{p}_\pi=0$ cross section, including both preemission and postemission, is plotted as a function of energy in Fig. 11. The overall change in appearance of $d\sigma/p_\pi{}^2dp_\pi$ from Fig. 7 is striking. Most of the difference is due to the nucleon preemission graph, although the (mostly destructive) interference of this graph with the postemission (isobar model) graphs is also important. Generally, at lower energies, the soft-pion production cross section is much enhanced by nucleon preemission.

Specific comments on Fig. 11 include the fol-

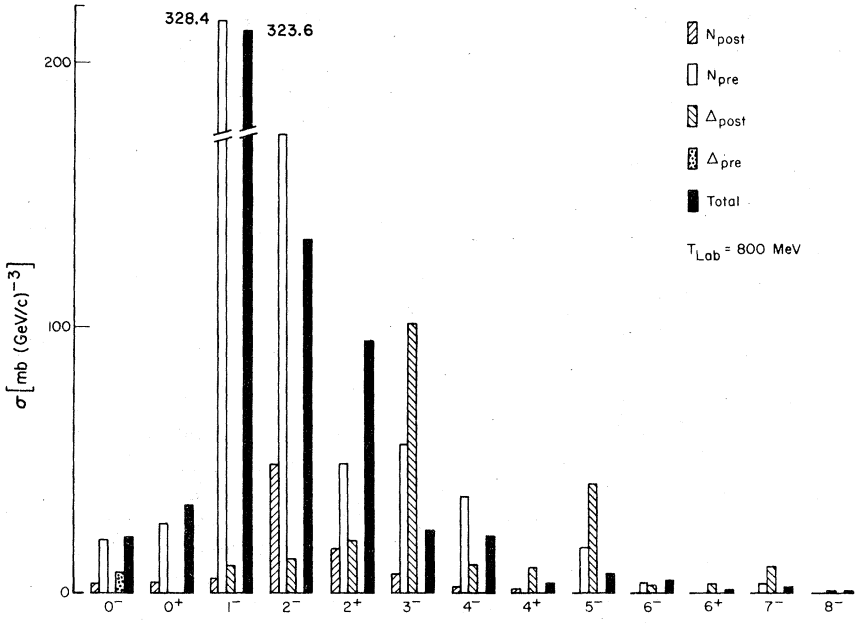

FIG. 10. Contributions of preemission and postemission graphs for individual partial waves for the $\vec{p}_\pi = 0$ $pp \to np\pi^+$ cross section at 800 MeV.

lowing.

(1) At 740 MeV, $|\Delta_{post}|^2$ is about 30% of $|N_{pre}|^2$, but these two contributions interfere destructively.

(2) The bump in $|N_{pre}|^2$ at 900 MeV (for which $T_{lab,\,pre} = 600$ MeV) reflects the resonance-like behavior in the elastic $NN \to NN$ $^1D_2$ final-state interaction. This behavior arises from the attraction provided by the unitary coupling to the inelastic $N\Delta$ channel (see Ref. 14).

(3) The bump in $|\Delta_{post}|^2$ at 600 MeV comes also from the sharp rise and fall of the $^1D_2$ inelastic $NN \to N\Delta$ amplitude.

(4) $|N_{pre}|^2$ is large at low energies because of a strong $^3S_1$ final-state interaction. The effect of this $^3S_1$ interaction, however, is rather model dependent. For one thing, the one-pion-exchange force which drives the Blankenbecler-Sugar integral equation that we solve for the isobar amplitudes (Fig. 4) predicts a $^3S_1$ phase shift quite different from experiment.[14] (This is almost certainly due to the neglect, so far, of short-range forces in the model). This suggests that using more realistic $^3S_1$ amplitudes would give a quite different curve for $|N_{pre}|^2$. If we simply compare the $|f(^3S_1)|^2 = \sin^2\delta(^3S_1)$, our model at 750 MeV ($T_{lab,\,pre} = 430$ MeV) gives a value some 15 times larger than experiment. (This explains why our predicted $\vec{p}_\pi = 0$ cross section, due mostly to nucleon preemission, is larger than that of Ref. 3). On the other hand, near threshold this situation is nearly reversed. The question of model dependence is further complicated by the off-shell dependence of our $NN \to NN$ amplitude, which can affect the predicted 1^- (i.e., $^3S_1$ final-state interaction) contribution to the cross section by as much as 50% in either direction, depending on energy.

(5) A "better" calculation of these preemission

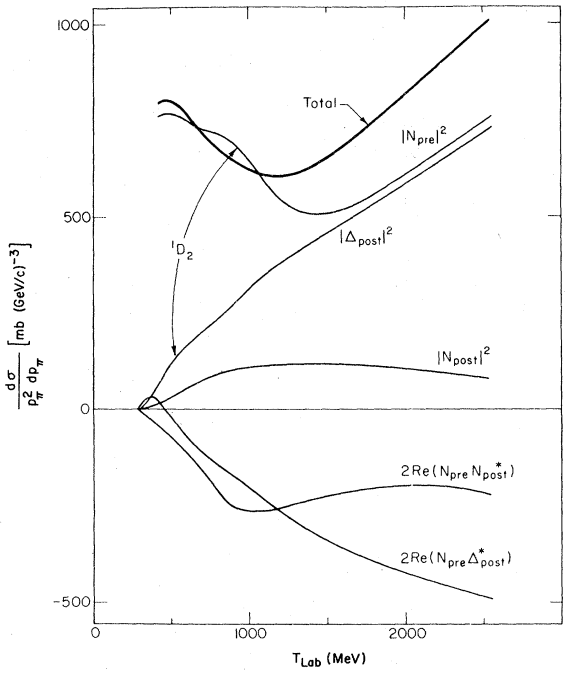

FIG. 11. Predicted "soft-pion" $pp \to np\pi^+$ cross section, including both preemission and postemission N' and Δ pole graphs.

graphs might therefore be to use our model only for the $N\Delta \to NN$ amplitudes and to take the $NN \to NN$ amplitudes from experiment (as in Ref. 3). If that were done, then $|\Delta_{post}|^2$ would be about equal to $|N_{pre}|^2$ at 740 MeV, instead of the 30% noted in (1) above.

The most important point about Fig. 11 is that, despite the inclusion of Δ-resonance contributions, the predicted $\vec{p}_\pi = 0$ cross section is still a factor of 3 or so smaller than experiment.

Before closing this section, we take this opportunity to illustrate the importance of using unitarized isobar amplitudes. Figure 12 shows the total $\vec{p}_\pi = 0$ cross section calculated above compared with a similar calculation which used the B_α (the Born terms, or driving terms, of Fig. 4) in place of the unitary T_α. This latter calculation might be called a Born approximation for $NN \to NN\pi$ (and it is very similar, for example, to the calculation of Ref. 21). The effects of using B_α's for T_α's in evaluating the C_J's are quite large, both in magnitude and energy dependence. It is interesting that the Born-approximation calculation *over*predicts the "soft-pion" cross section by about 50%. We feel there is an important lesson to be learned from Fig. 12, namely, that the near agreement of the Born approximation with the data point is misleading.

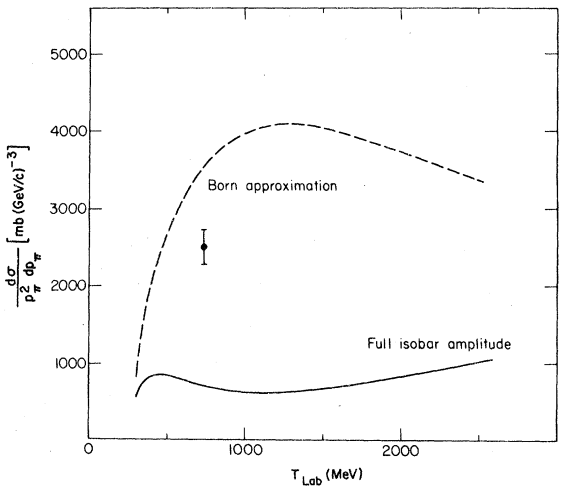

FIG. 12. Comparison of the Born-approximation calculation with the full calculation using the unitary isobar amplitudes obtained by solving the integral equations depicted in Fig. 4. The data point for this $pp \to np\pi^+$ cross section comes from Ref. 4.

VI. CONCLUSIONS

In accord with the suggestion made in Ref. 6, we have seen that the Δ postemission graph considerably increases the predicted $\vec{p}_\pi = 0$ cross section over the nucleon postemission graph. We have used a unitary, relativistic model to calculate the $NN \to NN'$ and $NN \to N\Delta$ isobar amplitudes needed in this isobar-model calculation. The isobar-model prediction is much smaller than experiment. Including the nucleon preemission graphs, in accord with the soft-pion theorem, brings the predicted cross section into much closer agreement. There is a lot of model dependence in the nucleon preemission contribution, but the major point we wish to make remains valid: The Δ-resonance "hard-pion" corrections to the soft-pion amplitude are very large in the $NN \to NN\pi$ process.

Since we nevertheless do not predict a $\vec{p}_\pi = 0$ cross section that agrees with experiment, let us note a number of points that could be considered.

(1) The πNN vertex used in this work is pseudoscalar coupling rather than pseudovector, as would be properly required by the soft-pion theorem. For the basically nonrelativistic nucleons involved here, we do not feel this would make significant numerical changes.

(2) Perhaps when the model of Ref. 13 is extended to include short-range forces in the Born (driving) terms, the $NN \to NN$ amplitudes needed for the nucleon-pole graphs may be quite different. It is unlikely that this will improve agreement with experiment, since using experimental NN amplitudes instead of our model amplitudes would probably lower the predicted cross section. [See comment (4) at the end of the previous section].

(3) The P_{11} πN input used in our isobar model can be improved (see Fig. 7 of Ref. 13). However, since σ' is so close to the πN threshold, we feel that this also would not make much difference.

(4) Perhaps the most likely reason for the remaining discrepancy with experiment is that more complicated dynamical mechanisms for pion production are needed. For instance, the internal emission graph shown in Fig. 1(d) may also be important for the $\vec{p}_{\pi=0}$ kinematical situation.

ACKNOWLEDGMENTS

We acknowledge useful conversations with a number of our colleagues on various aspects of this problem. In addition we wish to thank Michael Scadron also for his constant encouragement and Mario Schillaci for uncovering a copy of the computer program used for the calculations reported in Ref. 3. We also thank the Clinton P. Anderson Meson Physics Facility (LAMPF) for making available their VAX computing facilities. The work of J.D. and R.R.S. was supported by the U.S. Department of Energy. The work of W.M.K. was supported in part by the U.S. National Science Foundation.

*Present address: Department of Physics and Astronomy, University of Massachusetts, Amherst, Massachusetts 01002.

[1]S. L. Adler, Phys. Rev. 139, B1638 (1965); S. L. Adler and Y. Dothan, *ibid.* 151, 1267 (1966).
[2]F. E. Low, Phys. Rev. 110, 974 (1958); E. Nyman, *ibid.* 170, 1628 (1968).
[3]C. T. Grant, M. E. Schillaci, and R. R. Silbar, Phys. Rev. 184, 1737 (1969).
[4]D. R. F. Cochran, P. N. Dean, P. A. M. Gram, E. A. Knapp, E. R. Martin, D. E. Nagle, R. B. Perkins, W. J. Shlaer, H. A. Thiessen, and E. D. Theriot, Phys. Rev. D 6, 3085 (1972).
[5]R. A. Arndt, private communication.
[6]M. E. Schillaci and R. R. Silbar, Phys. Rev. D 2, 1220 (1970).
[7]S. Mandelstam, Proc. R. Soc London Ser. A: 244, 491 (1958).
[8]L. Michelotti, Phys. Rev. D 17, 185 (1978).
[9]P. Nuthakki and R. A. Uritam, Phys. Rev. D 6, 3233 (1972).
[10]G. K. Greenhut and G. W. Intemann, Phys. Rev. D 14, 764 (1976).
[11]P. Nuthakki and R. A. Uritam, Phys. Rev. D 8, 3196 (1973).
[12]W. M. Kloet, R. R. Silbar, R. Aaron, and R. D. Amado, Phys. Rev. Lett. 27, 1643 (1977).
[13]W. M. Kloet and R. R. Silbar, Nucl. Phys. A338, 281 (1980).
[14]R. R. Silbar and W. M. Kloet, Nucl. Phys. A338, 317 (1980).
[15]For a field-theoretic approach, see M. G. Olsson and E. T. Osypowski, Nucl. Phys. B101, 136 (1975).
[16]For a dispersion-theoretic approach, see M. D. Scadron and L. R. Thebaud, Phys. Rev. D 9, 1544 (1974).
[17]M. D. Scadron and L. R. Thebaud, Phys. Rev. D 8, 2190 (1973).
[18]J. T. MacMullen and M. D. Scadron, Phys. Rev. D 20, 1069 (1979); 20, 1081 (1979).
[19]We follow the conventions of A. R. Edmonds, *Angular Momentum in Quantum Mechanics* (Princeton University Press, N.J., 1957), except that the Clebsch-Gordan coefficient is denoted by a two-level symbol with parentheses and a bar, as already seen in Eq. (2).
[20]For the *total* inelastic $NN \to NN\pi$ cross section, the Δ-resonance contribution is some 50 times larger than that due to the P_{11} quasiparticle (Ref. 12, and unpublished).
[21]E. Borie, D. Drechsel, and H. J. Weber, Z. Phys. 267, 393 (1974).